POLITECNICO DI TORINO
Repository ISTITUZIONALE

Assessing the dependence of li-Ion batteries capacity on load current frequency

(Article begins on next page)

20 April 2024

Assessing the Dependence of Li-Ion Batteries Capacity on Load Current Frequency

Yukai Chen*, Wenlong Wang*, Daniele Jahier Pagliari*, Enrico Macii†, Massimo Poncino*

*Department of Control and Computer Engineering, Politecnico di Torino, Turin, Italy

†Interuniversity Department of Regional and Urban Studies and Planning, Politecnico di Torino, Turin, Italy

Email: yukai.chen@polito.it, daniele.jahier@polito.it, massimo.poncino@polito.it

Abstract—Lithium-ion batteries are the most common chemistry thanks to their many desirable properties, such as high energy density and long lifetimes; however, they still exhibit several non-ideal properties common to other battery chemistries, such as rated capacity effect, capacity dependence on load variation, and recovery effects. In the last two decades, many works in the EDA community have focused on methods to characterize and model these non-idealities. In particular, for the rated capacity effect and the recovery effect, accurate models have been derived that allow tracking battery behaviour with a reasonable degree of fidelity. However, one effect that has not been thoroughly explored is how battery capacity is affected by the spectral properties of the load current and its frequency distribution. Some preliminary works analyzed this relation based only on the information provided by datasheets and lacked an experimental validation of the resulting models. We conduct experimental measurements to analyze this dependence between usable battery capacity and the frequency spectrum of load current in this work. Our measurements illustrate that this relation is much more sophisticated than the one extracted from datasheets information: it is not monotonic and exhibits a local maximum point that changes over time as the battery ages.

Index Terms—Batteries, Battery Model, Battery Discharge Measurement, State of Charge, Battery Non-idealities

I. INTRODUCTION

Lithium-ion batteries have become the most popular energy storage choice for products of virtually any scale, from small portable electronic devices to large-scale electrical energy systems [1]. Their popularity is due to desirable properties such as high power and energy density, long lifetimes, and good tolerance to broader temperature ranges, resulting in better figures of merit concerning other chemistries. Although the lithium-ion battery has many merits, it still has several non-ideal properties as a chemical-electrical unit [2]. The rated capacity effect, recovery effect, and capacity dependence on load variations are three primary non-idealities during the charging and discharging phases [3] should be considered in the design of power management. Battery models that incorporate these effects are essential to obtain meaningful results from the simulation of electrical energy systems of any scale. Power simulation is essential in the initial design phase for systems power assessment and optimization. The corresponding model's accuracy is the foundation of whether the simulation can yield accurate power assessment.

The first two of these non-idealities, the rated capacity effect (i.e., the dependence of the usable capacity of a battery versus the current discharge rate) and the recovery effect (i.e., the recovery of usable capacity in the periods of rest), have been widely studied and included in state-of-the-art models with a reasonable degree of accuracy concerning the corresponding physical phenomenon [4] [5]. Such of these models also account for a different type of dependency on load current, namely the dependence of capacity on load current *variations* [6]. There is indeed a significant impact on battery capacity between a constant current discharge (preferable) and a general load waveform with the same average current value. A variable load current, besides different ranges of current magnitudes, however, also imply different distribution in the frequency domain: slow vs. fast current variations might also impact battery efficiency. Therefore, the variation of the load current is not only limited to the time domain but also includes the variation of the current in the frequency domain. For instance, the battery in the Electric Vehicle (EV) undergoes erratic variations during repeated acceleration and deceleration in the urban road traffic environment provides less capacity than when EV is in the highway road environment.

In literature, many works proposed to split the load into high-frequency and low-frequency components, then feed them into high-power storage device (super-capacitor) and high-energy storage device (battery), individually, to compose the hybrid energy storage systems [7]. However, only a few works investigated the battery available capacity and load frequency dependence. The work [8] indicates the load frequency affects the battery deliverable capacity and includes this effect in a discrete-time battery model. The authors of [9] proposed a methodology to characterize the relationship between battery available capacity and the load frequency. The work [6] proposed a circuit equivalent battery model that accounts for battery capacity dependence on the load current variation in time and frequency domains. However, these works are only dependent on the data provided on the datasheet, and none of them have been validated by measurement experiments. The authors of [10] conducted the frequency domain Electrochemical Impedance Spectroscopy (EIS) measurements to fit the battery circuit equivalent model, while they only focus on the battery voltage and ignore the capacity dependence. To the best of our knowledge, no previous work has quantified this battery capacity dependence on load current frequency by measurements. In this work, we quantify this non-ideal discharge characteristic by actual measurement experiments.

II. BACKGROUND AND MOTIVATION

A. Battery Non-ideal Discharge Characteristics

The process of providing power from a battery as a power source is an electrochemical process. Regardless of battery type and chemistry, a battery is far from an ideal power source due to its chemical characteristics; the power it can deliver depends heavily on the charging and discharging current profiles. This section overviews the two most relevant non-ideal discharge properties of lithium-ion batteries: the rated capacity effect and the dependence on load variation. We omit the introduction of the recovery effect because this effect is considered almost negligible in lithium-ion batteries [3] [11].

1) Battery Capacity Dependence on Load Magnitude:
Rated capacity effect expresses the available battery capacity at different discharge current magnitudes; for a constant current discharge of a battery, the available battery capacity decreases as the discharge current increases.

The lithium-ion battery manufacture datasheet normally uses a set of voltage vs. capacity curves to represent the rated capacity as shown in Figure 1. Figure 1 refers to the Panasonic's lithium-ion battery NCR18650B. The available capacity is obtained when the cell voltage reaches the cut-off voltage (2.5V for this cell). Notice that this lithium-ion battery's available capacity dependence on discharge current is quite low, showing only a small improvement of 0.2C current (i.e., 3200mA $\times$ 0.2 = 640mA) compared to other discharge currents. It is also well known that the rated capacity effect of lithium-ion batteries is much smaller than that of primary batteries [3]. Therefore, lithium-ion battery is replacing the primary battery in many applications, as it is more stable and reliable than the primary battery.
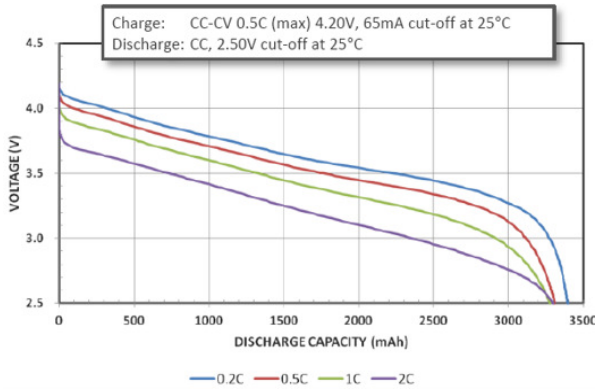

Fig. 1. Lithium-ion battery voltage vs. discharge current curves.

2) Battery Capacity Dependence on Load Variation: As an example of the variation over time, consider a periodic square wave I_{sw} alternating with a given constant duty cycle D between two current values I_1 (D) and I_2 ($1-D$) and a constant current I_{cons} with the average value $I_{avg} = D*I_1+(1-D)*I_2$ of the square wave current. The experiment discharging using I_{sw} shows a different result compared with using I_{cons}. The magnitude of the battery operation time difference shows a

positive correlation between I_1 and I_2, which is the larger difference between I_1 and I_2, the more evident the difference will be, the reason is that the higher I_1 activates, the more rated capacity effect occurs [3].

Besides the rated capacity effect, discharge load variation also influences the battery operation time from the frequency domain perspective. As stated in [8], the discharge current frequency affects the amount of charge the battery can deliver, the battery does not react instantaneously to load changes, but it shows considerable inertia, caused by the significant time constants that characterize electrochemical phenomena. As a further example based on the above periodic square wave I_{sw} example, the two current values I_1 (D) and I_2 ($1-D$) are fixed in this case, while a set of I_{sw} have different periods (frequencies). The results of this example are shown in [6], Figure 2 indicates that a battery has a longer operation time for constant current load profile, and the load profile with higher frequency reduces the battery operation time.
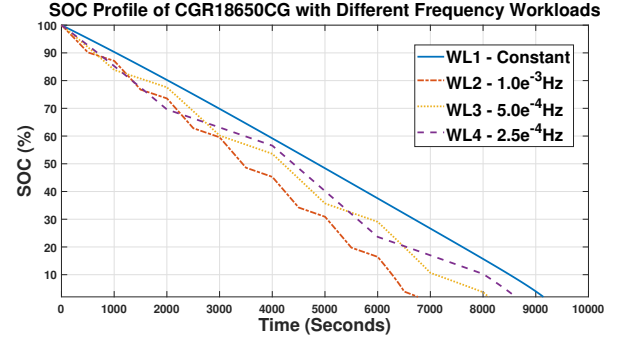

Fig. 2. Dependence of battery available capacity on load frequency [6].

B. Characterization and Modeling of Battery Non-Idealities

Existing works in the literature have tried to characterize the aforementioned non-ideal properties and build the battery models that can account for these non-ideal properties. The model of [8] accounts for the various non-idealities, including the load frequency variation effect; however, the work was not focused on how to identify the model parameters, so it does not provide hints on how to derive the model itself.
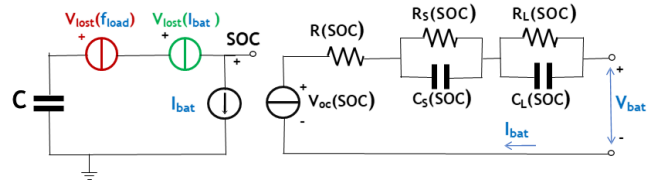
Fig. 3. The circuit equivalent battery model accounts for load variations.

The work [12] proposes a circuit equivalent battery model to overcome the low accuracy issue of the previous discrete-time model; it also can account for the transient battery voltage change, but without considering the non-ideal effects on battery capacity. [13] formalizes the battery modelling design space into a multi-level modelling approach by adding various non-ideal properties. Recently, [6] combines all the ideas

of previous works to develop one circuit equivalent battery model that can account for these two non-ideal effects as indicated in Figure 3. The two voltage generators $V_{lost}(I_{batt})$ and $V_{lost}(f_{load})$ on the left-hand side of the model represent the rated capacity effect $C(I_{batt})$ and the effect of load current variation $C(f_{load})$, which affect the battery available capacity (**SOC** node).

When using the battery model shown in Figure 3 in the simulation, $V_{lost}(I_{batt})$ is updated through, at each simulation time step Δt, Equation 1:

$$\Delta SOC(I_{batt}) = \frac{I_{batt} \times \Delta t}{C(I_{batt})} - \frac{I_{batt} \times \Delta t}{C_{nom}} \qquad (1)$$

where $C(I_{batt})$ is the dependence of battery available capacity on the battery discharge current. The dependence can be derived from the datasheet as described in [9] and C_{nom} is the nominal capacity. On the other hand, the dependence of battery available capacity on the discharge variation in the frequency domain is not an instantaneous quantity; therefore, the model applies the Short Time Fourier Transform (STFT) to compute load frequency components each time interval window. $V_{lost}(f_{load})$ is obtained by computing Equation 2:

$$\Delta SOC(f_{load}) = \sum_{i=1}^{N_{FFT}} \left(\frac{I_{batt}(i) \times \Delta t}{C(f_{load})} - \frac{I_{batt}(i) \times \Delta t}{C_{nom}} \right) \quad (2)$$

N_{FFT} is length of timing window adopted in STFT; $I_{batt}(i), i = 1, \ldots, N_{FFT}$ is a string of current values within a timing window; $C(f_{load})$ is the relation between capacity and load frequency. The method proposed in [9] shows that using the information in Figure 1 can derive the relation between discharge energy and current and the relation between discharge time and current. Then the relation between discharge power and current is computed based on the previous two relations. Using the power and current relation and the energy and current relation can draw *Ragone plot* [14]. The diagonals in the *Ragone plane* indicate the discharge time; the inverse of each discharge time represents a frequency. Thus the relation between energy and frequency is extracted; after converting energy to capacity, the $C(f_{load})$ is computed.

However, the estimation of the above circuit equivalent model's parameters is based on the available data provided in the battery datasheet. While this approach is reasonable for the rated capacity effect, for the dependence on load frequency, the extraction of the parameters is indirect [9] as described above. No direct measurements are carried out to validate this dependence extracted from the datasheet. Furthermore, extracting the dependence from the datasheet ignores the battery's aging issue because the discharge characteristics given in the datasheet, such as the curves shown in Figure 1, are generally measured by the fresh battery. For these reasons, the motivation of this work is to investigate whether the dependence of load current on the available battery capacity is consistent with the dependency extracted from the datasheet and the influence of the battery aging through a large number of experimental measurements.

III. Experimental Measurements and Analysis

A. Experimental Measurements Setup

The equipment adopted in our experiment can be divided into two main parts according to their functionality: the sampling and control parts. The former includes a battery gauge and a digital multimeter to track the battery's various electrical parameters. At the same time, the latter comprises a programmable electronic load and a programmable linear power supply that regulates the discharge and charge of the battery. Our experimental setup is shown in Figure 4.
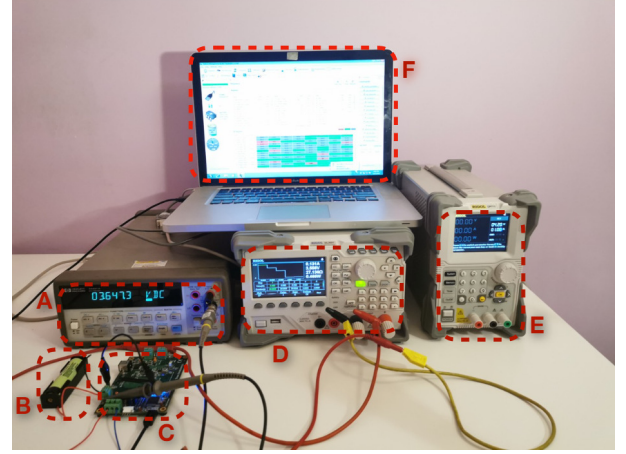

Fig. 4. Experimental setup: (A) HP 33401A Digital multimeter; (B) Panasonic NCR18650B Lithium-ion battery; (C) Texas Instruments Bq27z561 battery gauge; (D) RIGOL DL3021 programmable DC electronic load; (E) RIGOL DP711 programmable linear DC power supply; (F) BqStudio software user interface for the Texas Instruments Bq27z561 battery gauge.

We chose the widely used Panasonic NCR18650B Lithium-ion battery [15] in all our experiments, whose main electrical parameters are summarized in Table I.

TABLE I
Electrical specifications of the experimental batteries.

Rated Capacity	3200mAh
Nominal Voltage	3.6V
Cut-off voltage	2.5V

B. Experimental Measurements Parameters

This section reviews which parameters were used as variables in the exploratory analysis in our measurement experiments and their ranges.

1) Discharge Load Current Frequency: This parameter is the main parameter to be analyzed in this work. The frequency of the load current has been set as the frequency of a square wave generated by the programmable DC electronic load. We applied seven frequencies: 0.1Hz, 0.2Hz, 0.5Hz, 1Hz, 2Hz, 5Hz, and 10Hz. In the experiment, the chosen lithium-ion battery iterates the charge and discharge cycle by changing frequency in sequence from the lowest to the highest. In order to achieve high-resolution results, we set the sampling frequency of the measured data as 1Hz for all the experiments.

2) Discharge Load Current Magnitude: Concerning the current magnitude, we set the square wave to discharge current as a fixed 50% duty cycle and 1000mA average current for all the experiments. The high and low values of the square waveform are determined by observing that we cannot set the low value too small since the battery would perceive it as a relaxation interval rather than a discharge. Moreover, a too-small low swing value will imply a relatively sizeable high value, resulting in a more significant rated-capacity effect to weaken the observation of capacity dependence on load frequency measurements. Based on these considerations, we used [500mA, 1500mA] as extremes of the voltage swing.

3) Battery State of Charge (SOC): In this work, all the experiments rely on monitoring the battery SOC, which is done using the Bq27z561 battery gauge by Texas Instruments (TI), equipped with an EValuation Module (EVM) with an independent power source. The evaluation board of the gauge provides interfaces for connecting the battery and load device. The data captured by the gauge is transmitted to the PC via a Micro USB interface. All data are visualized by a software called BqStudio, which provided by TI.

The essential parameters in the monitoring of SOC are the initial and final SOC levels. To avoid voltage variations in the proximity of the theoretical extremes (100% and 0% SOC), we assume the initial SOC to be 90% and 30% as the final value. The latter is particularly critical, as when battery SOC approaches lower SOC levels, the discharge characteristics become unstable, and the battery voltage drops sharply. To ensure that the measurement results of each experiment are in a stable state of battery discharge, we thus consider the discharge procedure as terminated when SOC reaches 30%.

4) Battery State of Health (SOH): A new battery's capacity and rate characteristics do not stay unchanged as it ages. Changes can be summarized as a loss of chemical capacity and impedance increase. Due to aging effects, the usable capacity decreases along with time. For this reason, we set battery SOH as a quantity monitored in our experiments. It is calculated automatically by the battery gauge as Q_{max}/Q_{nom}. The Q_{max} is the available battery capacity of a used battery, and Q_{nom} is the new battery nominal capacity in standard conditions, which assume (1) that a CC-CV charging protocol charges the battery at 25°C environmental temperature, and (2) the charging current in the CC phase is set as 1A. In practice, the battery SOH reaches 80% is considered the end of life; however, our experiments set the SOH is 85% as our explorative lower bound to avoid forcing the battery in extreme conditions and causing some unstable data be measured.

C. Experimental Workflow

A single experiment comprises three phases described hereafter; the experiments execute these three phases with different load current frequencies described in the previous section.

1) Discharge Phase: Discharge parameters have been discussed in Section III-B. During the discharge procedure, the battery gauge monitors SOC, discharge current, and battery voltage; these are sent to the PC through a Micro USB interface and visualized on the PC by BqStudio. In the meantime, BqStudio records all these data into a log file.

2) Charge Phase: The battery is charged by CC/CV mode with 1A 4.2V configuration using DP711 DC power supply. The charge process will be terminated when the battery SOC reaches 90%. As in the discharge phase, the charging process is monitored by the battery gauge (SOC) and digital multi-meter (current and voltage) to guarantee the battery is under CC/CV charging protocol, and the charging phase is terminated when the gauge detects battery SOC reaches 90%.

3) Relaxation Phase: After each charge or discharge phase, the battery requires a relaxation period to reach a relatively stable voltage level to get ready for a new discharge procedure. Based on suggestions from the equipment manufacturers, the relaxation time is chosen as 2 hours for both charge and discharge phases.

The flow of a given experiment proceeds according to the following schedule:

1) Charge phase until the battery reaches 90% SOC;
2) Relaxation phase.
3) Discharge phase by a given frequency until a 30% SOC
4) Relaxation phase

After each charge and discharge cycle, we track the battery SOH, and the schedule is iterated until the battery SOH decreases to 85% as described above.

D. Experimental Measurements Results

1) Discharge Time vs. Discharge Current Frequency: The first data we extract concerns the relation between the discharge time of the battery (90 to 30% SOC) versus the frequency of the load frequency. Results are summarized in Figure 5 in the box-plot format in order to account for the variation among the six different instances of Panasonic NCR18650B cells used in the experiments. The data shown in Figure 5 is referred to results of SOH=94% cycle; more measurements related to battery SOH are presented in the following subsection. The box in Figure 5 corresponding to each frequency indicates the maximum, minimum, and mean discharge time of these six different battery cells.
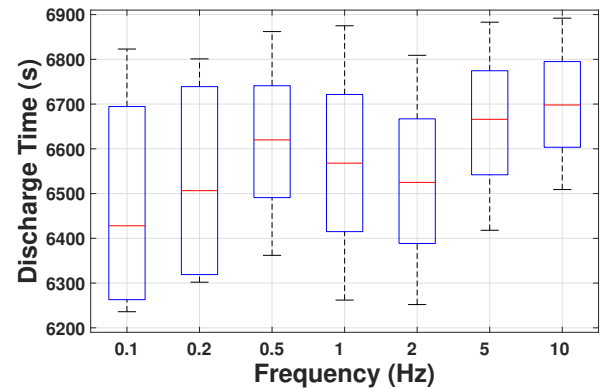
Fig. 5. Battery discharge time to 30% SOC vs load frequency.

The figure 5 shows that the frequency affects the discharge time, although it does not reveal a well-defined trend. The

most important conclusion is that the discharge time tends to be generally longer for higher frequencies than lower ones. Intuitively this should be because the battery acts as a sort of low-pass filter, and apparently, higher frequencies start to be filtered out since it is well-known that a battery handles better constant currents than variables one, load current with frequencies higher than a few Hertz are assimilated as a constant load profile. Numerically speaking, we observed a difference of about 4.5% discharge time in the average values, while the maximum difference can reach around 10%.

Concerning lower frequencies, the discharge time tends to increase up to a local maximum (in SOH=94% case, 0.5Hz), to start decreasing again until the higher frequencies are present again. This non-monotonic behaviour in the lower frequency ranges might be due to the structure of the equivalent impedance of the battery. The impedance of the lithium-ion battery measured by EIS shown in the work [10] reveals a similar variation trend, and the impedance also follows a non-monotonic behaviour.

2) Battery SOH vs Discharge Time-Frequency Dependence: When repeated the experimental schedule on one single battery cell many times, the experiments result in a loss of battery capacity and a consequent decrease of the SOH over time. We observed an interesting relationship between battery SOH and the discharge time-frequency dependence described previously, illustrated in Figure 6.
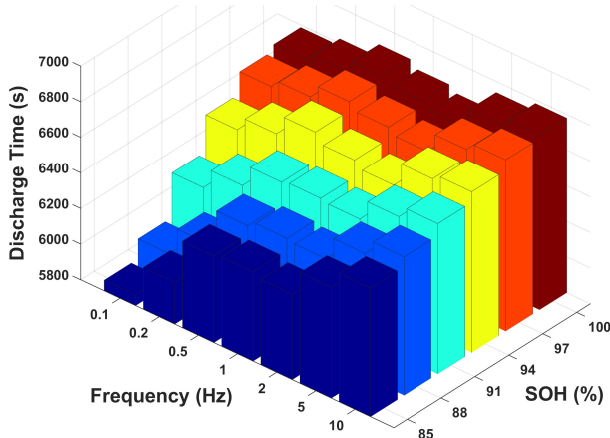

Fig. 6. Battery discharge time vs. load frequency under different SOHs.

The first evident characteristic is clearly visible from the plot. The dependency on frequency becomes more and more evident as the battery ages. While for a fresh one (100% SOH), the difference between best and worst discharge times appears negligible, as the aging progresses, it becomes more sizable. For a battery with 85% SOH, the difference in average discharge time among the six different battery cells between the min/max frequencies is now around 9.4%, notice that this quantity is 4.5% at SOH = 94%, as indicated above.

Another attractive characteristic is that the *pattern* in the low-frequency range differs depending on the SOH (from 0.1Hz to 1Hz shown in Figure 6), while it tends to be similar

in the high-frequency range (from 2Hz to 10Hz shown in Figure 6). This phenomenon can be explained by analyzing the relationship between load frequency and battery impedance. Figure 7, taken from [16], shows the results of a C/10 rate discharge cycling test. It shows tremendous impedance change due to aging at the low-frequency part (which is most important for DC discharge), while impedance for frequencies higher than 1 Hz is less sensitive to the battery SOH. Figure 6 illustrates that there is no significant change in the curves' shape of the cases with frequency larger than 1 Hz from cycle 1 to cycle 100.
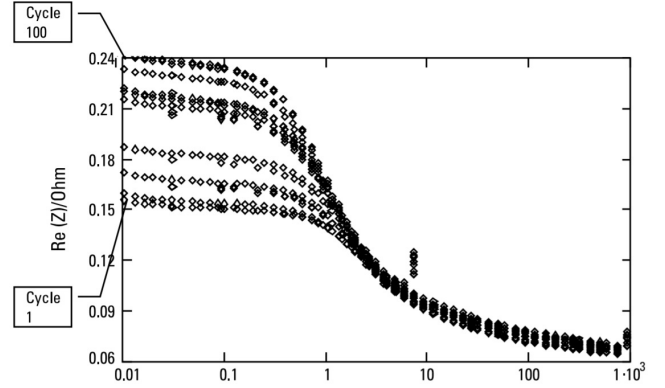

Fig. 7. Impedance spectra measured from 10mHz to 1kHz after each 10 cycles of a 100-cycle test using Lithium-ion battery [16]

IV. DEPENDENCE ON LOAD FREQUENCY COMPARISON OF MEASUREMENTS WITH DATASHEET EXTRACTION

In the process of conducting power simulation, the ability of the battery model to respond correctly to the load frequency determines the accuracy of the power estimation during the simulation [17]. The critical step in building the battery model that can accurately account for the load frequency dependence as shown in Figure 3 is computing the $C(f_{load})$ as described in Equation 2. In this section, we show the comparison of $C(f_{load})$ extracted through the battery datasheet with the $C(f_{load})$ obtained by our experimental measurement results in section IV, and illustrate the importance of battery aging on the $C(f_{load})$ computation.

According to the methodology of extracting the relationship between battery available capacity and load frequency proposed in the work [9], we derived the $C(f_{load})_{Datasheet}$ based the Figure 1 as shown in Equation 3:

$$C(f_{load})_{Datasheet} = -6.914 \times f_{load}^{0.2324} + 4.139 \quad (3)$$

Deriving $C(f_{load})_{Measure}$ is more straightforward than extraction from datasheet data. By performing a curve fitting with the data shown in Figure 6, it yields $C(f_{load})_{Measure}$ for different SOH cases. Notice the measurements results correspond to the SOC operating range from 90% to 30%, which means only consuming 60% of the nominal capacity. To compare with the case of using the datasheet data, we thus ideally scaled up this 60% capacity to 100% nominal capacity. Since the load current profile is known, the discharge

time data in Figure 6 is easily converted to the capacity ($Time \times Current$), then $Capacity \times \dfrac{100\%}{60\%}$ scaled up to obtain the battery available capacity. This is not a rigorous scaling up, but we do this to show the difference between the two methods to obtain $C(f_{load})$. Our future work will consider measurements of the discharge from 100% to 0%.

Due to the space limitation, we only show below two Equations 4, 5 derived from the two extremes cases of the measurement results, i.e., SOH=100% and SOH=85%. As shown in Figure 6, the dependence of battery discharge time on the load frequency is not monotonically increasing. The simple power function fitting method used in datasheet extraction is no longer available; thus, we chose the rational number function fitting method to obtain the following two equations.

$$C(f)_{Measure}^{SOH=100\%} = \frac{3.16 \times f^3 - 3.71 \times f^2 + 0.03 \times f + 3.07}{f^3 - 1.11 \times f^2 - 0.08 \times f + 1.02}$$
(4)

$$C(f)_{Measure}^{SOH=85\%} = \frac{3.08 \times f^3 - 0.56 \times f^2 + 2.67 \times f + 1.78}{f^3 - 0.03 \times f^2 - 0.68 \times f + 0.68}$$
(5)

where f represents f_{load} as Equation 3 due to the line space.

Figure 8 shows a visual comparison of the three dependence obtained above in the same coordinate plane; it indicates the dependence extracted from the datasheet and measurements have no overlap, and the capacity changing trends are entirely different. The curve represents the dependence derived from the datasheet ends about $5 \times 10^{-4} Hz$ due to the limited data provided in the datasheet, e.g., Figure 1 solely provide four different discharge currents, and the maximum one is 2C, which limits the maximum frequency can extract [9]. On the other hand, the minimum frequency used in the measurement experiment is only $0.1 Hz$, which leaves no overlap between the derived dependence from the datasheet and measurements. In future work, the measurement experiment needs to build a complete set of frequencies to explore the results of the frequency overlap interval with the datasheet.
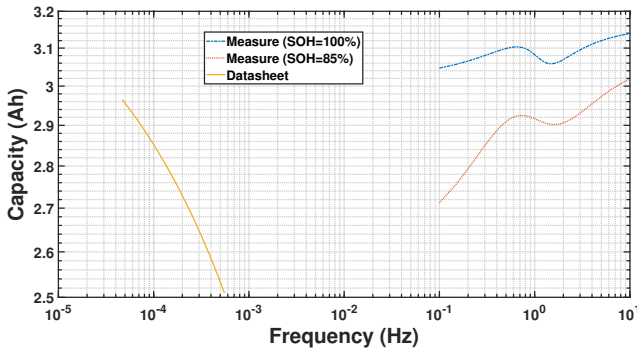

Fig. 8. Dependence comparison between measurements and datasheet.

There is another critical finding from Figure 8. Using the dependence ($C(f_{load})$) derived from datasheet to do power simulation in previous work [6], when the load frequency is higher than the maximum frequency that datasheet can extract

through method in [9], the available battery capacity is set as the capacity corresponds to the maximum frequency that datasheet can extract. However, the measurements indicate that it is an apparent underestimation; Figure 8 shows the capacity related to the frequency range $[10^{-1} Hz - 10^1 Hz]$ is higher than the $5 \times 10^{-4} Hz$ (the maximum frequency that the datasheet can extract). Figure 8 indicates a more complete dependence characterization requires the experimental measurements with a broader frequency range.

V. Conclusion

This work analyzes the battery capacity dependence on load profile frequency through actual experimental measurements. The measured experimental results calibrate the dependence between battery capacitance and load frequency indicated in the previous works extracted from the datasheet. The most noteworthy finding in this work is that this dependence is not monotonically decreasing with increasing load frequency, as previous works have shown, for the available battery capacity. Instead, it increases and then decreases, having a locally optimal frequency for the battery. Furthermore, our work further reveals that this dependence is not fixed throughout the whole battery life and that it changes as the battery capacity ages, showing that the optimum frequency becomes progressively larger. The future works will conduct a complete set of frequencies in the measurements and incorporate the battery capacity dependence on load current frequency into the exiting circuit equivalent battery model to capture this effect during the simulation; SOH information should also be considered to develop a lifelong model.

References

[1] G. Zubi, R. Dufo-López, M. Carvalho, and G. Pasaoglu, "The lithium-ion battery: State of the art and future perspectives," Renewable and Sustainable Energy Reviews, vol. 89, 2018, pp. 292–308.

[2] V. Muenzel, A. F. Hollenkamp, A. I. Bhatt, J. de Hoog, M. Brazil, D. A. Thomas, and I. Mareels, "A comparative testing study of commercial 18650-format lithium-ion battery cells," Journal of The Electrochemical Society, vol. 162, no. 8, 2015, p. A1592.

[3] Y. Chen, W. Wang, D. J. Pagliari, E. Macii, and M. Poncino, "Assessing the impact of sensor-based task scheduling on battery lifetime in iot devices," IEEE Transactions on Instrumentation and Measurement, 2021.

[4] M. R. Jongerden and B. R. Haverkort, "Which battery model to use?" IET software, vol. 3, no. 6, 2009, pp. 445–457.

[5] A. Hausmann and C. Depcik, "Expanding the peukert equation for battery capacity modeling through inclusion of a temperature dependency," Journal of Power Sources, vol. 235, 2013, pp. 148–158.

[6] Y. Chen, E. Macii, and M. Poncino, "A circuit-equivalent battery model accounting for the dependency on load frequency," in Proceedings of the Conference on Design, Automation & Test in Europe. European Design and Automation Association, 2017, pp. 1177–1182.

[7] S. Hajiaghasi, A. Salemnia, and M. Hamzeh, "Hybrid energy storage system for microgrids applications: A review," Journal of Energy Storage, vol. 21, 2019, pp. 543–570.

[8] L. Benini, G. Castelli, A. Macii, E. Macii, M. Poncino, and R. Scarsi, "Discrete-time battery models for system-level low-power design," IEEE Transactions on Very Large Scale Integration (VLSI) Systems, vol. 9, no. 5, 2001, pp. 630–640.

[9] Y. Chen, E. Macii, and M. Poncino, "Frequency domain characterization of batteries for the design of energy storage subsystems," in 2016 IFIP/IEEE International Conference on Very Large Scale Integration (VLSI-SoC). IEEE, 2016, pp. 1–6.

[10] P. Kollmeyer, A. Hackl, and A. Emadi, "Li-ion battery model performance for automotive drive cycles with current pulse and eis parameterization," in 2017 IEEE transportation electrification conference and expo (ITEC). IEEE, 2017, pp. 486–492.

[11] S. Narayanaswamy, S. Schlueter, S. Steinhorst, M. Lukasiewycz, S. Chakraborty, and H. E. Hoster, "On battery recovery effect in wireless sensor nodes," ACM Transactions on Design Automation of Electronic Systems (TODAES), vol. 21, no. 4, 2016, pp. 1–28.

[12] M. Chen and G. A. Rincon-Mora, "Accurate electrical battery model capable of predicting runtime and iv performance," IEEE transactions on energy conversion, vol. 21, no. 2, 2006, pp. 504–511.

[13] Y. Kim, D. Shin, M. Petricca, S. Park, M. Pontino, and N. Chang, "Computer-aided design of electrical energy systems," in 2013 IEEE/ACM International Conference on Computer-Aided Design (IC-CAD). IEEE, 2013, pp. 194–201.

[14] T. Christen and M. W. Carlen, "Theory of ragone plots," Journal of power sources, vol. 91, no. 2, 2000, pp. 210–216.

[15] PANASONIC, "NCR18650B lithium-ion battery cell datasheet," https://www.batteryspace.com/prod-specs/NCR18650B.pdf, 2019.

[16] Y. Barsukov and J. Qian, Battery power management for portable devices. Artech house, 2013.

[17] D. Baek, Y. Chen, A. Bocca et al., "Battery-aware operation range estimation for terrestrial and aerial electric vehicles," IEEE Transactions on Vehicular Technology, vol. 68, no. 6, 2019, pp. 5471–5482.